Universal Parameters for Carbon Nanotube Network-Based Sensors: Can Nanotube Sensors Be Reproducible?

Byung Yang Lee,[†] Moon Gyu Sung,[†] Joohyung Lee,[†] Ku Youn Baik,[†] Young-Kyun Kwon,[‡] Moon-Sook Lee,[§] and Seunghun Hong[†,⊥,*]

[†]Department of Physics and Astronomy, Seoul National University, Seoul 151-747, Korea, [‡]Department of Physics and Research Institute for Basic Sciences, Kyung Hee University, Seoul 130-701, Korea, [§]Samsung Advanced Institute of Technology, Yongin-si, Gyeonggi-do 446-712, Korea, and [⊥]Department of Biophysics and Chemical Biology, Seoul National University, Seoul 151-747, Korea

ABSTRACT Carbon nanotube (CNT) network-based sensors have been often considered unsuitable for practical applications due to their unpredictable characteristics. Herein, we report the study of universal parameters which can be used to characterize CNT network-based sensors and make their response predictable. A theoretical model is proposed to explain these parameters, and sensing experiments for mercury (Hg^{2+}) and ammonium (NH_4^+) ions using CNT network-based sensors were performed to confirm the validity of our model.

KEYWORDS: carbon nanotube · sensor · mechanism · adsorption · Langmuir isotherm

Carbon nanotubes (CNTs) have been extensively studied due to their remarkable electrical and mechanical properties.[1] Especially, sensors with field-effect transistor (FET) structures using CNTs and CNT networks as a channel have been widely utilized for various sensing applications.[2] However, sensors with CNT channels suffer from irregularity in their individual electrical and mechanical properties. This irregularity originates from diverse sources, for example, from the different synthesis process of CNTs,[3,4] chirality distribution,[5] and variation of device contact resistance.[6] This inherent irregularity of the individual CNT devices results in unpredictable and highly irregular behavior of CNT-based sensors, impeding their practical applications and commercialization.[7,8] In many cases, one cannot even reproduce the sensing results reported in the literature quantitatively.

Herein, we report the study of the universal parameters which enable us to quantify and even predict the sensing behaviors of diverse CNT network-based sensors. To explain these parameters, we propose a theoretical model where the target molecules are adsorbed onto the CNT surfaces *via* the Langmuir isotherm process and the conductance of the sensor transducer changes *via* capacitive coupling or charge transfer. The validity of the model has been confirmed by sensing experiments on mercury (Hg^{2+}) and ammonium (NH_4^+) ions using a number of CNT network-based sensors. Considering that the unpredictable characteristics of CNT network-based sensors have been holding back their practical applications, this work should be a major breakthrough in CNT network-based sensor research and open various practical applications such as environmental safety and medical diagnostics.

RESULTS AND DISCUSSION

The studies reported herein are motivated by the need to overcome the irregular electrical properties of CNT network-based sensors. We utilized multichannel CNT network-based sensors to figure out the sensor responses in a controlled manner. Figure 1 shows a schematic diagram depicting the experimental setup and theoretical model for the CNT network-based sensors. The sensor responses of 16 CNT sensors were measured simultaneously using a multichannel measurement system, and a liquid gate profile was measured using a Ag/AgCl reference electrode.

For the theoretical model, we assume that analyte *A* in bulk solution was adsorbed onto a finite number of binding sites *B* on the CNT surfaces following a Langmuir isotherm model (Figure 1). In the Langmuir isotherm model, it is assumed that analyte molecules in solution bind to a finite number of *binding sites* on solid substrates, and the analyte molecules in solution and those bound to the binding sites form an equilibrium. The binding sites can be different adsorption sites on the CNT sensor surface

* Address correspondence to seunghun@snu.ac.kr.

Received for review November 11, 2010 and accepted May 20, 2011.

Published online May 26, 2011
10.1021/nn103056s

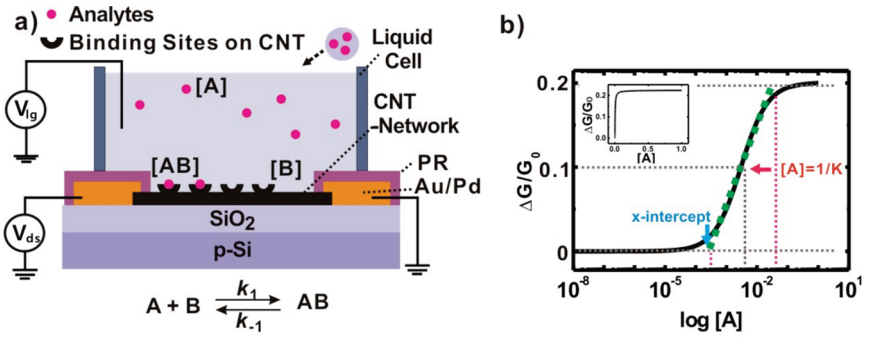

Figure 1. Schematic diagram depicting the measurement setup and our theoretical model. (a) CNT network channel is connected by source and drain electrodes. The electrodes were covered with photoresist (PR) to minimize the leakage currents through the solution. A liquid cell was formed to confine the solution. (b) For theoretical modeling, we assume that analytes *A* get adsorbed to the binding sites *B* on the CNT surface *via* the Langmuir isotherm process with equilibrium constant *K* (=k_1/k_{-1}), and only those adsorbed molecules *AB* generate the sensor response, $\Delta G/G_0$. $\Delta G/G_0$ *vs* log[*A*] is plotted according to the Langmuir isotherm (inset: $\Delta G/G_0$ *vs* [*A*]). The sensor response has a linear response region whose center value is at [*A*] = 1/*K*.

depending on the type of the CNT sensor. For example, the binding sites on common CNT-based gas sensors are gas adsorption sites on bare CNT surfaces.[9−11] In the case of specific biosensors based on CNT FETs, specific receptor molecules fixed on CNT surfaces work as binding sites.[12] Let [*A*], [*B*], [*AB*], and $[B]_{max}$ represent the concentration of analytes in bulk solution, the surface density of binding sites on CNT networks, the surface density of adsorbed analyte molecules, and the maximum surface density of binding sites on CNT networks, respectively. Then, the surface density of adsorbed analytes can be expressed following a Langmuir isotherm (Figure 1b) like

$$[AB] = [B]_{max} \times \frac{[A]}{[A] + 1/K} \quad (1)$$

with equilibrium constant $K = k_1/k_{-1}$, where k_1 and k_{-1} are the association and dissociation constants, respectively.[13] Since CNTs respond to analytes only within the distance of Debye length in ionic solutions due to the screening effect,[14] we can assume that the sensor response of our sensors is mostly due to the analytes adsorbed onto the CNT channels.

Although a previous report showed that charge carriers can transport ballistically in *individual* CNTs,[15] CNT *network-based channels* are usually composed of multiple CNTs overlapping on each other to form junctions. In this case, we can expect rather diffusive charge transport due to the short mean free paths. Thus, we can ignore any coherent gating effect and assume that the current change ΔI in the channel is affected by the adsorbed analyte concentration [*AB*] on CNT surfaces *via* electric coupling like

$$\Delta I = G_L \times \Delta V_A \approx g_L V_{ds} \times \frac{\Delta q_A}{C_0} = g_L V_{ds} \times \frac{q_A [AB]}{C_0} = g_L V_{ds} \times \frac{q_A}{C_0} [B]_{max} \times \frac{[A]}{[A] + 1/K} \quad (2)$$

where G_L represents the liquid gate transconductance; ΔV_A the liquid potential change around the CNTs caused by the adsorbed analyte molecules; g_L the normalized transconductance defined by $g_L \approx G_L/V_{ds}$; Δq_A the total electric charge contributed by the adsorbed analyte molecules to the CNTs; q_A the electric charge contributed by the unit surface density of the adsorbed analyte molecules to the CNTs; and C_0 is the coupling constant between the analyte molecules and CNT surfaces.

Previous reports show the two most common mechanisms about how charged analytes near the CNT surface can affect the conductance of CNT network channels: electric field gating[16] and direct charge transfer.[17] In the case of electric field gating, charged analytes near CNTs may exert electric fields on the CNT channels, giving a gating effect just like in field-effect transistors. In this case, C_0 represents the capacitive coupling between the charged analytes and the CNT channels. On the other hand, adsorbed analytes may directly transfer electrical charges onto the CNTs *via* direct contact. In this case, C_0 is determined by the electronegativity of the adsorbed analytes with respect to that of CNTs. In both cases, q_A and C_0 are determined by the type of analytes and should not be affected by the CNT device structures.

From eq 2, the sensor response, defined as the conductance change ($\Delta G = \Delta I/V_{ds}$) with respect to initial conductance G_0, becomes

$$\frac{\Delta G}{G_0} = \left(\frac{g_L}{G_0}\right) \times \frac{q_A}{C_0} [B]_{max} \times \frac{[A]}{[A] + 1/K} \quad (3)$$

It is worth mentioning several important aspects of this equation. First, g_L/G_0 represents the electrical characteristics of the CNT device and should be independent of the analyte species. It can be estimated by simple electrical measurement on the CNT device without performing actual sensing experiments. Second, $(q_A/C_0)[B]_{max}$ and *K* represent the *electric coupling*

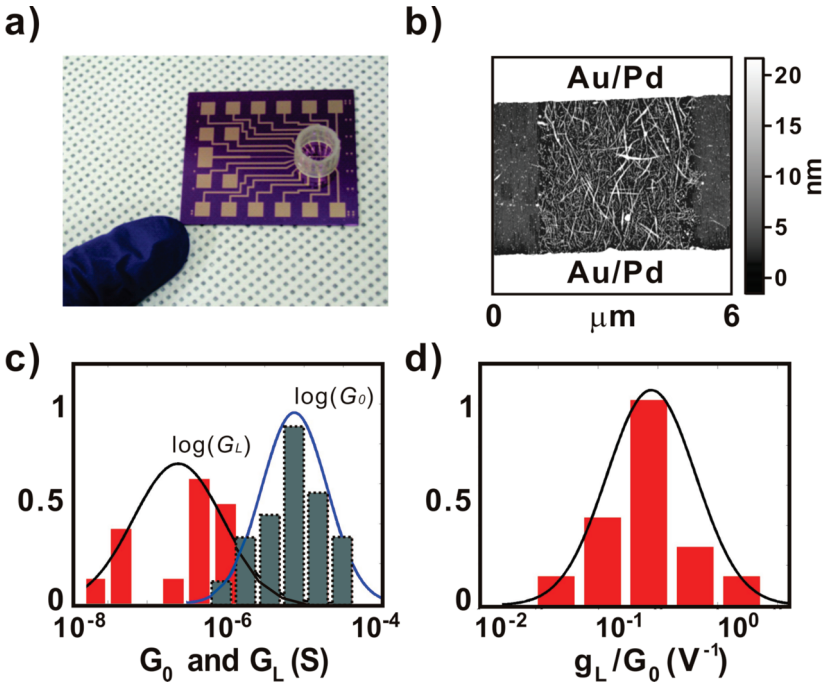

Figure 2. Characterization of CNT newtork-based sensors. (a) Optical micrograph of a chip containing 16 CNT network-based sensors. (b) AFM topography image of a typical CNT device without PR passivation layer on Au electrodes. The surface density of the adsorbed single-walled CNTs (swCNTs) is ~4 #/μm^2. The unit #/μm^2 represents the number of CNTs in a unit substrate area of 1 μm^2.[19] (c) Distribution of initial conductance G_0 and liquid gate transconductance G_L for 21 CNT network-based sensors. G_0 exhibited a log-normal distribution, while G_L exhibited a rather random distribution. (d) Distribution of the normalized transconductance g_L/G_0, a characteristic for each CNT device. It exhibited a log-normal distribution.

and the *adsorption* properties of the analyte molecules onto CNT-based sensor surfaces, respectively. Considering $[B]_{max}$ as a constant, both can be determined only by the analyte type and do not depend on the CNT device structures or nanotube chirality.

In a previous report, we showed that the sensor response can be expressed in linear form to logarithmic concentration in certain range of concentration.[18] In this linear response region, we can write

$$\frac{\Delta G}{G_0} \sim \frac{1}{4\log_{10} e}\left(\frac{g_L}{G_0}\right) \times \frac{q_A}{C_0}[B]_{max} \times [\log_{10}[A] + \log_{10}(e^2K)] \quad (4)$$

If we set $x = \log_{10}[A]$ and $y = \Delta G/G_0$, the equation becomes

$$y \sim \alpha[x - \gamma] \quad (5)$$

where

$$\alpha\left(\equiv \frac{1}{4\log_{10} e}\left(\frac{g_L}{G_0}\right) \times \frac{q_A}{C_0}[B]_{max}\right)$$

and $\gamma(\equiv -\log_{10}(e^2K))$ represent the slope and x-intercept of the sensor response graph, respectively, as indicated in Figure 1b.

These variables were verified with a multichannel measurement system, which enabled us to apply identical environmental change to 16 CNT network-based sensors on a single substrate (Figure 2a). The atomic force microscopy (AFM) topography image in Figure 2b shows one of the CNT network channels. Here, the CNT channel consists of a rather uniform monolayer of CNTs resulted from the "self-limiting" mechanism during CNT adsorption, where the already-adsorbed CNTs impede the adsorption of additional CNTs. This "self-limiting" mechanism is advantageous for obtaining rather uniform arrays of CNT channels.[13,19] However, it also should be mentioned that previous works show that the surface density of adsorbed CNTs prepared by our process has some distribution around the monolayer coverage following the log-normal distribution.[20,21] Such a distribution may cause a slight variation of surface binding site density and channel conductance of the CNT devices. Furthermore, even for the devices with uniform CNT density, the conductance of the devices shows some distribution due to the variation of the network connectivity.[2]

Since we utilized single-walled CNT (swCNT) solution containing both semiconducting and metallic CNTs, the assembled CNT network channels consisted of both semiconducting and metallic current paths.[17] Our multichannel CNT junctions exhibited a log-normal distribution in G_0, which is typical for percolating conductive networks (Figure 2c).[20,22] In the case of the liquid gate transconductance G_L, they exhibited about one order wider distribution. The junction exhibited a negative liquid gate transconductance at a small gate bias, which is a typical p-type semiconducting behavior of CNT channels under ambient conditions. The gating

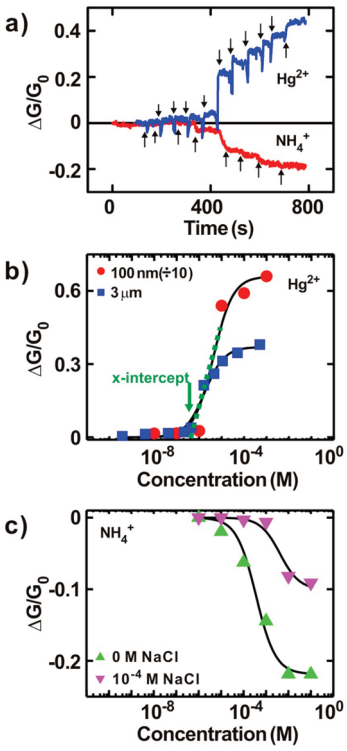

Figure 3. Sensor response of CNT network-based sensors. (a) Typical real-time detection signal of CNT-based sensor to Hg^{2+} and NH_4^+ ions. (b) Sensor response $\Delta G/G_0$ with respect to logarithmic concentration of Hg^{2+} ions for different channel width. The channel width varied from 3 μm to 100 nm with 1/10 reduction of the data values for 100 nm to fit in the graph. (c) Sensor response $\Delta G/G_0$ with respect to logarithmic concentration of NH_4^+ ions for different salt concentration. The sensor response was measured with or without 10^{-4} M of NaCl in the solution. The sensor response curves in (b) and (c) are fitted well to a Langmuir adsorption model (solid line), and the linear response regions are fitted well in almost the same range for each species (green dotted line).

effect data show the on−off current ratio of 1.7 with a significant off current due to the metallic paths in the CNT network (Figure S4 in Supporting Information). Figure 2d shows the normalized transconductance g_L/G_0, which is a characteristic parameter for each CNT device, independent of the target molecular species. It has a log-normal distribution over a rather broad range due to some variations in CNT network channels, such as the number of semiconducting paths and CNT network connectivity.

For actual sensing experiments, multiple sensors were exposed to the analyte with the concentrations of 35.3 pM to 5.23 mM in the case of mercury ions (Hg^{2+}, $HgCl_2$ in DI water) and 1 μM to 100 mM in the case of ammonium ions (NH_4^+, NH_4OH in DI water). The sensor response of each sensor, defined as the conductance change ΔG with respect to the initial conductance G_0, was monitored and recorded simultaneously from multiple sensors using the multichannel measurement system. Figure 3a shows a typical real-time detection signal of Hg^{2+} and NH_4^+ ions. In the case of Hg^{2+} detection, exposure to Hg^{2+} increases the conductance due to the strong redox reaction between Hg^{2+} ions and CNTs.[13] This redox reaction takes electrons away from CNTs, which increases the number of hole carriers in CNTs and thus raises the conductance of CNTs. On the other hand, NH_4^+ is well-known to decrease the conductance of CNTs.[9,23]

Figure 3b,c shows the sensor response $\Delta G/G_0$ of typical sensors with respect to logarithmic concentrations of Hg^{2+} and NH_4^+, respectively. Here, the sensor response shows large dependence on experimental conditions even for a given analyte species. For example, our sensors with a *narrower* CNT network channel exhibited a *larger* sensor response to Hg^{2+} as reported previously (Figure 3b).[18] This can be explained by the dominating semiconducting current paths in narrower CNT network channels.[24,25] On the other hand, NH_4^+ in the 0.1 mM NaCl solution generates much smaller sensor response compared with that in deionized water (Figure 3c). Presumably, the salt ions may screen out the electric field from the ammonium and reduce the gating effect on the CNTs. Furthermore, we found that each of our sensors exhibits quite a different sensor response in the same experimental condition as reported previously by many other researchers.

However, we could also figure out somewhat coherent behaviors in our sensing measurements. First of all, sensor response data in Figure 3b,c are in a similar form and are fitted very well by a Langmuir isotherm-like equation such that $\Delta G/G_0$ is proportional to $[A]/([A] + 1/K)$ as proposed in our theoretical model (eq 3). Here, K is the equilibrium constant (Figure 1b).[18] Second and most interestingly, for the analyte, CNT network-based sensors appear to respond within the similar concentration. Specifically, our sensors exhibit large sensor responses in the range of 0.22−16 μM for Hg^{2+} and 10^{-5}−10^{-3} M for NH_4^+. Note, this range depends only on the analyte species and not on any other conditions such as CNT network channel width (Figure 3b) or salt concentration (Figure 3c). These two consistent characteristics support our theoretical hypothesis that analytes adsorbed on the CNT surface form a Langmuir isotherm and semiconducting CNTs in our sensor channels can respond only to nearby charges and change their conductance.

These characteristics can be validated by comparing the experimental results with the prediction of the model. The measured sensor responses from various CNT sensors were plotted to the logarithmic concentration of analytes, and the linear regions were fitted using eq 5 (Figure S5 in Supporting Information). The equilibrium constant K is estimated from the x-intercept $\gamma \equiv -\log_{10}(e^2K)$ of the fitting curve. Figure 4a displays the distribution of the x-intercept γ values obtained from various devices. These fitted γ values fall into a narrow range around a certain values for a given analyte species. From each value of the x-intercept γ,

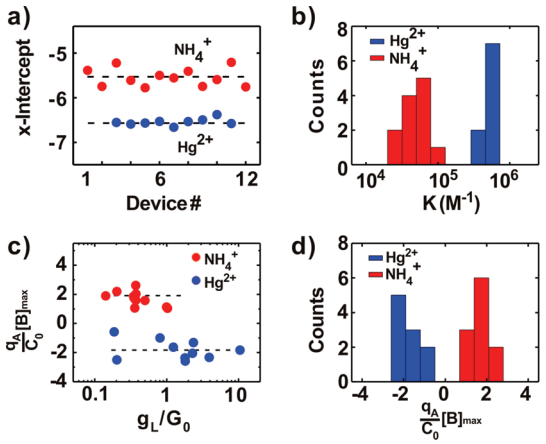

Figure 4. Estimation of the equilibrium constant K and the coupling parameter $q_A[B]_{max}/C_0$. (a) Graph showing the x-intercept values obtained from the fitted line in the linear response regions of the sensor response curves. (b) Distribution of the equilibrium constant K estimated from sensor response curves of different CNT-based sensors, which are sharply peaked at 4.8×10^5 and 5.2×10^4 M^{-1} for Hg^{2+} and NH_4^+, respectively. (c) Graph showing the coupling parameter $q_A[B]_{max}/C_0$ with respect to the device parameter g_L/G_0. (d) Distribution of the coupling parameter $q_A[B]_{max}/C_0$ estimated from the sensor response of different CNT-based sensors, which are sharply peaked at −1.9 and 1.8 V for Hg^{2+} and NH_4^+ ions, respectively.

the corresponding equilibrium constant K can be obtained, and the distributions of K values for two different analytes are depicted in Figure 4b. It shows that they are narrowly distributed around a peak value for each target analyte. The evaluated values are $K = 4.8 \times 10^5$ M^{-1} for Hg^{2+} and $K = 5.2 \times 10^4$ M^{-1} for NH_4^+. These are similar with those of previous works[13,18] which are in the range of measured distribution in Figure 4b. It also should be noted that K value itself may vary under different experimental conditions, such as temperature, which might have, in part, caused some distributions of measured K values (Figure 4b).[26]

This result is consistent with our model because, for the same analyte, the devices should have a similar adsorption behavior in regards to the target molecules regardless of the device structures. Even though there was an earlier study showing a small variation of K values based on the observation using only a few CNT FETs,[7] here we show for the first time that K is a constant value evaluated statistically by measurements using a large number of network-based CNT sensors and even under various conditions. Until now, CNT network-based sensors have exhibited a large variation in their responses, which makes them extremely difficult, if not impossible, to use for industrial applications. Our result shows that different CNT sensors can have a *universal parameter* such as K independent of the variations of its device characteristics such as conductance or transconductance.

This result also provides us an important insight about the sensitivity or detection limit of CNT network-based sensors. Assume that, due to the electrical noise, the device conductance G of our CNT-based sensor is limited by a noise fluctuation of N_G. Then, from eq 5, the minimum meaningful sensor response $\Delta G_{min}/G_0$ of this sensor is

$$\frac{N_G}{G_0} \cong \frac{\Delta G_{min}}{G_0} = \left(\frac{g_L}{G_0}\right) \times \frac{g_A}{C_0}[B]_{max} \times \frac{[A_{min}]}{[A_{min}] + 1/K} \quad (6)$$

where $[A_{min}]$ represents the detection limit, the minimum concentration of the target analyte which can be detected by the sensor. If we solve it for $[A_{min}]$, one can obtain

$$[A_{min}] = \frac{1}{K} \times \frac{1}{g_L \frac{q_A}{C_0}[B]_{max}/N_G - 1} \quad (7)$$

As expected, one can reduce the detection limit of the CNT sensors by increasing the transconductance g_L as well as reducing the noise level. It also clearly shows that the detection limit is linearly proportional to the $1/K$. This is because CNT sensors respond only to the analyte molecules near the CNT surface. Thus, one should consider the adsorption behavior of the analyte molecules onto the CNT surface when designing sensitive sensors. For example, in many cases, the CNT surfaces are functionalized with receptor molecules which can bind specifically to a target molecular species. One can further improve the sensitivity of CNT sensors by coating with receptor molecules with large K values.

It is worth discussing our model at a very low concentration limit like $[A] \ll 1/K$. One of the major advantages of CNT sensors is its high sensitivity, and it is very important to model the sensor responses at a very low concentration. However, in a practical FET-based sensor device, its detection limit is usually determined by its noise level N_G. At the low concentration limit of $[A] \ll 1/K$, the size of sensor response ΔG usually becomes comparable to that of device noise N_G. Thus, the measurement results of sensor responses in this range often become unreliable, and it is not appropriate to describe the data using our model. On the other hand, our work shows that a more practical solution in achieving a *reliable sensor response at a low concentration* is the functionalization of CNT surfaces with receptor molecules with a low $1/K$ value so that the linear sensor response region is shifted toward the lower concentration. In fact, we could achieve a femtomolar level sensitivity by functionalizing the CNT surfaces with receptor molecules which had a low $1/K$ value.[27,28] We also would like to mention a practical issue in achieving a low detection limit.[29] Our model assumed an equilibrium state of the sensor systems. However, at an extremely low concentration limit, one should consider the long sensor response time to reach such an equilibrium state when estimating its detection limit of the sensors as reported previously.[29]

We can also estimate the coupling parameter $(q_A/C_0)[B]_{max}$ from the slope α of the fitting curve and

the measured device parameter g_L/G_0 through $(q_A/C_0)[B]_{max} = \alpha/[(1/4\log_{10}e)(g_L/G_0)]$. Figure 4c shows the estimated coupling parameter $(q_A/C_0)[B]_{max}$ for the devices with different values of device parameter g_L/G_0. Significantly, it turns out that for the same analyte, the estimated $(q_A/C_0)[B]_{max}$ values are almost identical from CNT devices with different g_L/G_0. It verifies the validity of our theoretical model.

Figure 4d shows the distributions of the coupling parameter $(q_A/C_0)[B]_{max}$ for two different analytes measured by various CNT devices. They are sharply peaked around −1.9 V for Hg^{2+} and 1.8 V for NH_4^+. It indicates that the coupling parameter $(q_A/C_0)[B]_{max}$ is mainly determined by analyte species even for CNT network-based sensors with different initial conductance and transconductance values as predicted in our theoretical model.

In our model (eq 3), the sensor response $\Delta G/G_0$ at the analyte concentration $[A]$ is determined by three major parameters: device parameter g_L/G_0, coupling parameter $(q_A/C_0)[B]_{max}$, and equilibrium constant K. We demonstrated that CNT sensors exhibited almost identical values of $(q_A/C_0)[B]_{max}$ and K for the analyte. The normalization method for nanowire-based sensors using liquid gate transconductance introduced by Ishikawa *et al.* is also consistent with the linear relationship between sensor response and one of our parameters, g_L/G_0.[30] With these three parameters, one can now quantitatively predict the sensor response of versatile CNT-based sensors before performing actual sensing experiments.

In summary, the CNT network-based sensors with different device characteristics (*e.g.*, conductance, transconductance, *etc.*) exhibited almost identical values of the equilibrium constant K and the coupling parameter $(q_A/C_0)[B]_{max}$ for the analyte. These two parameters can be universal parameters which can be used to quantify the sensing behaviors of versatile CNT network-based sensors independent of different device structures or nanotube chiralities. Furthermore, we can quantitatively predict the sensor response using our model and the measured device parameter g_L/G_0, which should enable reliable sensor signal processing. Our work should provide an important theoretical framework in understanding the mechanism of CNT network-based sensors and, eventually, allow us to produce reliable and predictable sensor devices for practical applications.

METHODS

We have utilized a previously reported directed assembly method to fabricate our swCNT network-based devices (Figure S1 in Supporting Information).[21,22] Two different shapes of CNT network patterns were fabricated. One has the width of 3 μm and the length of 2 μm, and the other has the width of 100 nm and the length of 2 μm. First, 3 μm wide line patterns of photoresist (AZ5214) and 100 nm wide line patterns of e-beam resist (PMMA) were created on SiO_2 substrate *via* photolithography and e-beam lithography, respectively.[18,24] When the patterned substrate was placed in the hydrophobic octadecyltrichlorosilane (OTS) solution (1:500 v/v in hexane), OTS molecules were patterned on SiO_2 substrate. After removing the resist, the patterned substrate was dipped into CNT solution (0.05 mg mL^{-1}) in dichlorobenzene. In this case, the OTS molecular layer blocked the CNT adsorption, and the CNTs were assembled only onto the bare SiO_2 region. Metal electrodes were formed by photolithography, successive thermal evaporation of 10 nm Pd and 20 nm Au, and lift-off process. Afterward, the electrodes were passivated with photoresist (AZ5214) to impede any electrochemical reaction with the bulk solution at the surface of the electrodes. Then, a polypropylene liquid cell was attached around the CNT array region to keep the liquid environment containing electrolytes. The final sensor chip had an array of 16 CNT network-based sensors. The sensor responses of multiple CNT sensors were measured simultaneously using a multichannel measurement system (Figures S2 and S3 in Supporting Information). The measurement system consists mainly of a sample holding jig, power supply, switch array, multiplexer, and a digital multimeter (DMM). A liquid gate profile of our CNT devices was measured using a Ag/AgCl reference electrode (Figure S4 in Supporting Information).[16,31] A bias voltage (V_{ds}) of 0.1 V was applied between the source and drain electrodes for sensor response and liquid gate measurements. To get liquid gate transconductance, the liquid-gated voltage V_{lg} was swept cyclically between −0.3 and 0.3 V with the source−drain voltage of $V_{ds} = 0.1$ V. The gate voltage sweep was restricted to a rather low bias voltage to minimize possible electrochemical reaction and leakage currents between the reference electrode and the solution.[31,32]

Acknowledgment. This work was supported by the NRF grant (No. 2011-0000390) and Samsung Electronics. S.H. acknowledges support from the Converging Research Center Program (No. 2010-k001138) and the WCU program.

Supporting Information Available: Supplementary methods and additional details on fabrication method, electrical characterization, functionalization methods, and supplementary figures. This material is available free of charge *via* the Internet at http://pubs.acs.org.

REFERENCES AND NOTES

1. Baughman, R. H.; Zakhidov, A. A.; de Heer, W. A. Carbon Nanotubes—The Route toward Application. *Science* **2002**, *297*, 787–792.
2. Lee, B. Y.; Seo, S. M.; Lee, D. J.; Lee, M.; Lee, J.; Cheon, J.-H.; Cho, E.; Lee, H.; Chung, I.-Y.; Park, Y. J.; *et al.* Biosensor System-on-a-Chip Including CMOS-Based Signal Processing Circuits and 64 Carbon Nanotube-Based Sensors for the Detection of a Neurotransmitter. *Lab Chip* **2010**, *10*, 894–898.
3. Xia, Y.; Ma, Y.; Xing, Y.; Mu, Y.; Tan, C.; Mei, L. Growth and Defect Formation of Single-Wall Carbon Nanotubes. *Phys. Rev. B* **2000**, *61*, 11088–11092.
4. Teo, K. B. K.; Lee, S.-B.; Chhowalla, M.; Semet, V.; Binh, V. T.; Groening, O.; Castignolles, M.; Loiseau, A.; Pirio, G.; Legagneux, P.; *et al.* Plasma Enhanced Chemical Vapour Deposition Carbon Nanotubes/Nanofibres—How Uniform Do They Grow? *Nanotechnology* **2003**, *14*, 204–211.
5. Arnold, M. S.; Green, A. A.; Hulvat, J. F.; Stupp, S. I.; Hersam, M. C. Sorting Carbon Nanotubes by Electronic Structure Using Density Differentiation. *Nat. Nanotechnol.* **2006**, *1*, 60–65.

6. Appenzeller, J.; Knoch, J.; Derycke, V.; Martel, R.; Wind, S.; Avouris, P. Field-Modulated Carrier Transport in Carbon Nanotube Transistors. *Phys. Rev. Lett.* **2002**, *89*, 126801.
7. Abe, M.; Murata, K.; Ataka, T.; Matsumoto, K. Calibration Method for a Carbon Nanotube Field-Effect Transistor Biosensor. *Nanotechnology* **2008**, *19*, 045505.
8. Nair, P. R.; Alam, M. A. Screening-Limited Response of NanoBiosensors. *Nano Lett.* **2008**, *8*, 1281–1285.
9. Kong, J.; Franklin, N. R.; Zhou, C. W.; Chapline, M. G.; Peng, S.; Cho, K. J.; Dai, H. J. Nanotube Molecular Wires as Chemical Sensors. *Science* **2000**, *287*, 622–625.
10. Li, J.; Lu, Y.; Ye, Q.; Cinke, M.; Han, J.; Meyyappan, M. Carbon Nanotube Sensors for Gas and Organic Vapor Detection. *Nano Lett.* **2003**, *3*, 929–933.
11. Maeng, S; Moon, S.; Kim, S.; Lee, H.-Y.; Park, S.-J.; Kwak, J.-H.; Park, K.-H.; Park, J.; Choi, Y.; Udrea, F.; *et al.* Highly Sensitive NO_2 Sensor Array Based on Undecorated Single-Walled Carbon Nanotube Monolayer Junctions. *Appl. Phys. Lett.* **2008**, *93*, 113111.
12. Besteman, K.; Lee, J.-O.; Wiertz, G. M.; Heering, H. A.; Dekker, C. Enzyme-Coated Carbon Nanotubes as Single-Molecule Biosensors. *Nano Lett.* **2003**, *3*, 727–730.
13. Kim, T. H.; Lee, J.; Hong, S. Highly Selective Environmental Nanosensors Based on Anomalous Response of Carbon Nanotube Conductance to Mercury Ions. *J. Phys. Chem. C* **2009**, *113*, 19393–19396.
14. Kim, J. P.; Lee, B. Y.; Hong, S.; Sim, S. J. Ultrasensitive Carbon Nanotube-Based Biosensors Using Antibody-Binding Fragments. *Anal. Biochem.* **2008**, *381*, 193–198.
15. Javey, A.; Guo, J.; Wang, Q.; Lundstrom, M.; Dai, H. Ballistic Carbon Nanotube Field-Effect Transistors. *Nature* **2003**, *424*, 654–657.
16. Rosenblatt, S.; Yaish, Y.; Park, J.; Gore, J.; Sazonova, V.; McEuen, P. L. High Performance Electrolyte Gated Carbon Nanotube Transistors. *Nano Lett.* **2002**, *2*, 869–872.
17. Bradley, K.; Briman, M.; Star, A.; Grüner, G. Charge Transfer from Adsorbed Proteins. *Nano Lett.* **2004**, *4*, 253–256.
18. Lee, M.; Lee, J.; Kim, T. H.; Lee, H.; Lee, B. Y.; Park, J.; Jhon, Y. M.; Seong, M.-J.; Hong, S. 100 nm Scale Low-Noise Sensors Based on Aligned Carbon Nanotube Networks: Overcoming the Fundamental Limitation of Network-Based Sensors. *Nanotechnology* **2010**, *21*, 055504.
19. Im, J.; Huang, L.; Kang, J.; Lee, M.; Lee, D. J.; Rao, S. G.; Lee, N. K.; Hong, S. "Sliding Kinetics" of Single-Walled Carbon Nanotubes on Self-Assembled Monolayer Patterns: Beyond Random Adsorption. *J. Chem. Phys.* **2006**, *124*, 224707.
20. Rammal, R.; Lemieux, M.-A.; Tremblay, A.-M. S. Comment on "ε Expansion for the Conductivity of a Random Resistor Network". *Phys. Rev. Lett.* **1985**, *54*, 1087.
21. Lee, M.; Im, J.; Lee, B. Y.; Myung, S.; Kang, J.; Huang, L.; Kwon, Y.-K.; Hong, S. Linker-Free Directed Assembly of High-Performance Integrated Devices Based on Nanotubes and Nanowires. *Nat. Nanotechnol.* **2006**, *1*, 66–71.
22. Lee, B. Y.; Heo, K.; Bak, J. H.; Cho, S. U.; Moon, S.; Park, Y. D.; Hong, S. Scalable Assembly Method of Vertically-Suspended and Stretched Carbon Nanotube Network Devices for Nanoscale Electro-Mechanical Sensing Components. *Nano Lett.* **2008**, *8*, 4483–4487.
23. Bradley, K.; Gabriel, J. C. P.; Briman, M.; Star, A.; Gruner, G. Charge Transfer from Ammonia Physisorbed on Nanotubes. *Phys. Rev. Lett.* **2003**, *91*, 218301.
24. Lee, M.; Noah, M.; Park, J.; Seong, M.-J.; Kwon, Y.-K.; Hong, S. Textured Network Devices: Overcoming Fundamental Limitations of Nanotube/Nanowire Network-Based Devices. *Small* **2009**, *5*, 1642–1648.
25. Lee, M.; Baik, K. Y.; Noah, M.; Kwon, Y.-K.; Lee, J.-O; Hong, S. Nanowire and Nanotube Transistors for Lab-on-a-Chip Applications. *Lab Chip* **2009**, *9*, 2267–2280.
26. Wang, Z.; Yu, X.; Pan, B.; Xing, B. Norfloxacin Sorption and Its Thermodynamics on Surface-Modified Carbon Nanotubes. *Environ. Sci. Technol.* **2010**, *44*, 978–984.
27. Kim, T. H.; Song, H. S.; Jin, H. J.; Lee, S. H.; Namgung, S.; Kim, U. K.; Park, T. H.; Hong, S. "Bioelectronic Super-Taster" Device Based on Taste Receptor-Carbon Nanotube Hybrid Structures, *Lab Chip* 2011, DOI: 10.1039/C0LC00648C.
28. Kim, T. H.; Lee, S. H.; Lee, J.; Song, H. S.; Oh, E. H.; Park, T. H.; Hong, S. Single-Carbon-Atomic-Resolution Detection of Odorant Molecules Using a Human Olfactory Receptor-Based Bioelectronic Nose. *Adv. Mater.* **2009**, *21*, 91–94.
29. Nair, P. R.; Alam, M. A. Theoretical Detection Limits of Magnetic Biobarcode Sensors and the Phase Space of Nanobiosensing. *Analyst* **2010**, *135*, 2798–2801.
30. Ishikawa, F.; Curreli, M.; Chang, H. K.; Chen, P. C.; Zhang, R.; Cote, R. J.; Thompson, M. E.; Zhou, C. A Calibration Method for Nanowire Biosensors to Suppress Device-to-Device Variation. *ACS Nano* **2009**, *3*, 3969–3976.
31. Minot, E. D.; Janssens, A. M.; Heller, I.; Heering, H. A.; Dekker, C.; Lemay, S. G. Carbon Nanotube Biosensors: The Critical Role of the Reference Electrode. *Appl. Phys. Lett.* **2007**, *91*, 093507.
32. Koh, J.; Yi, M.; Lee, B. Y.; Kim, T. H.; Lee, J.; Jhon, Y. M.; Hong, S. Directed Assembly of Carbon Nanotubes on Soft Substrates for Use as a Flexible Biosensor Array. *Nanotechnology* **2008**, *19*, 505502.